Transport of Divalent Transition-Metal Ions Is Lost in Small-Intestinal Tissue of *b*/*b* Belgrade Rats†

Martin Knöpfel,‡,§,|| Lin Zhao,‡ and Michael D. Garrick*,‡

Department of Biochemistry, SUNY, Buffalo, New York 14214, and Department of Clinical Pharmacology, University of Berne, 3010 Berne, Switzerland

Received June 14, 2004; Revised Manuscript Received December 3, 2004

ABSTRACT: Belgrade rats exhibit microcytic, hypochromic anemia and systemic iron deficiency due to a glycine-to-arginine mutation at residue 185 in a metal ion transporter of a divalent metal transporter/divalent cation transporter/solute carrier 11 group A member 2 or 3 (DMT1/DCT1/SLC11A2), a member of the natural-resistance-associated macrophage protein (Nramp) family. By use of rabbit duodenal tissue, a calcein fluorescence assay has previously been developed to assess transport of divalent metal ions across the small-intestinal brush border membrane (BBM). The assay was readily applied here to rat BBM to learn if it detects DMT1 activity. The results demonstrate protein-mediated transport across the BBM of all tested ions: Mn^{2+}, Fe^{2+}, and Ni^{2+}. Transport into BBM vesicles (BBMV) from (*b*/*b*) Belgrade rats was below the detection limit. BBMV of +/*b* origin had substantial activity. The kinetic rate constant for Ni^{2+} membrane transport for +/*b* BBMV was within the range for normal rabbit tissue. Vesicles from +/*b* basolateral membranes (BLM) showed similar activity to BBMV while *b*/*b* BLM vesicles (BLMV) lacked transport activity. Immunoblots using isoform-specific antibodies demonstrated that intestinal levels of *b*/*b* DMT1 were increased compared to +/*b* DMT1, reflecting iron deficiency. Immunoblots on BBMV indicated that lack of activity in *b*/*b* vesicles was not due to a failure of DMT1 to localize to the BBMV; an excess of specific isoforms was present compared to +/*b* BBMV or duodenal extracts. Immunoblots from BLMV also exhibited enrichment in DMT1 isoforms, despite their distinct origin. Immunofluorescent staining of thin sections of *b*/*b* and +/*b* proximal intestines confirmed that DMT1 localized similarly in mutant and control enterocytes and showed that DMT1 isoforms have distinct distributions within intestinal tissue.

Trace elements are essential for enzyme activity, immune defense, radical reactions, and oxygen transport. The supply of transition metals in our body, particularly iron, may depend on the activity of divalent metal transporter/divalent cation transporter/solute carrier 11 group A member 2 (DMT1/DCT1/Nramp2/SLC11A2). The function of this transporter was identified by expression cloning in oocytes of *Xenopus laevis* (*1*). It was ubiquitously expressed and is responsible for the uptake of iron from the gut by the brush border membrane (BBM) (*2*−*4*). It is also critical for iron egress from the endosomal vesicle in transferrin-receptor (TfR)-mediated transport (*3*, *5*, *6*). DMT1-mediated transport activity is present in the small-intestinal epithelial cells (enterocytes) of the duodenum and upper jejunum where maximum trace element transport is found.

Homozygous Belgrade (*b*/*b*) rats manifest systemic iron deficiency (*7*, *8*) due to a mutation (*3*) that disrupts the transport function of DMT1. Thus the rats exhibit microcytic, hypochromic anemia inherited as an autosomal recessive trait (*8*, *9*). Bypassing transferrin (Tf) delivery of iron in reticulocytes (*10*) demonstrated that there was a defect in the cellular uptake of iron via Tf as also suggested by Bowen and Morgan (*11*). The defect was proximal to mitochondrial iron utilization (*12*) and localized to release of iron in the endosome (*5*). Iron supplementation does not cure the anemia in *b*/*b* rats (*13*) consistent with the insight that TfR-mediated iron transport was hindered (*5*). Non-Tf-bound iron uptake

† This project was supported by the National Research Initiative of the USDA Cooperative State Research, Education and Extension Service, Grant No. 2001-35200-10723 to M.D.G.

* To whom correspondence should be addressed. Department of Biochemistry, SUNY, 140 Farber Hall, Buffalo, NY 14214-3000, USA. Phone: (716) 829-3926. Fax: (716) 829-2725. E-mail: mgarrick@buffalo.edu.

‡ SUNY at Buffalo.

§ University of Berne.

|| Present address: TraceChem, Belpstrasse 41, CH-3007 Berne, Switzerland.

[1] Abbreviations: DMT1, divalent metal transporter 1; DCT1, divalent cation transporter 1; Nramp2, natural-resistance-associated macrophage protein 2; SLC11A2 or 3, solute carrier 11 group A member 2 or 3; TfR, transferrin receptor (specifically TfR1); *b*/*b*, homozygous phenotypically anemic Belgrade rat; Tf, transferrin; G185R, glycine-to-arginine mutation at residue 185 of DMT1/DCT1/Nramp2; IREG1, iron-regulated protein 1; MTP1, metal-transporter protein 1; SLC40A1, solute carrier 40 group A member 1; +/*b*, heterozygous Belgrade rat; BBM, brush border membrane; BBMV, brush border membrane vesicle(s); BLM, basolateral membrane; BLMV, basolateral membrane vesicle(s); IRE, iron-responsive element; EDTA, ethylenediaminetetraacetic acid; PMSF, phenylmethane sulfonyl fluoride; AEBSF, 4-(2-aminoethyl)-benzenesulfonyl fluoride hydrochloride; AA, ascorbic acid; E_a, activation energy; EGTA, ethylene dioxy-bis-(ethylenenitrilo)-tetraacetic acid; Hepes, N-(2-hydroxyethyl)-piperazine-N′-2-ethanesulfonic acid.

10.1021/bi048768+ CCC: $30.25
Published on Web 02/10/2005

(*14*, *15*) and manganese uptake (*16*) were also impaired. Just after discovery of the function of DMT1 (*1*), a glycine-to-arginine mutation at residue 185 (G185R) missense mutation was detected in the DMT1 gene on chromosome 7 of Belgrade rats (*3*); remarkably identical with the mutation (*2*) in microcytic (*mk*/*mk*) mice (*17*−*19*).

Transport of iron into the proximal small intestine depends on the function of an array of proteins involved in several steps across the epithelial cell layer. Ferrireductase activity (*20*, *21*) is involved in reduction of Fe^{3+} to Fe^{2+} prior to DMT1-mediated transport into the enterocytes where excess iron might be stored in ferritin. Ferroportin/iron-regulated protein 1 (IREG1)/metal-transporter protein 1 (MTP1)/solute carrier 11 group A member 3 (SLC11A3), now SLC40A1 (*22*−*24*), is regarded as essential at the basolateral side for export with hephaestin (*25*) plus ceruloplasmin (*26*) contributing to reoxidation to gain affinity to Tf for distribution throughout the body. It remains unclear in this context to what extent the G185R mutation affects intestinal iron transport in Belgrade rats. Only homozygous (*b*/*b*) animals are anemic, but they still seem to be able to take up at least a certain amount of iron. The remaining iron uptake could be due to a ferric transporter (*27*), heme iron uptake (*28*), a backup ferrous iron transport system, or residual activity of DMT1 (*3*, *29*−*31*). Although *b*/*b* homozygotes are severely affected, +/*b* rats do not manifest any deficiency phenotypically.

The present study investigated the divalent metal ion transport capacity of *b*/*b* and +/*b* Belgrade rats in the small-intestinal BBM and basolateral membrane (BLM) using Mn^{2+}, Fe^{2+}, and Ni^{2+}. Measurements were performed with calcein loaded BBM vesicles (BBMV) to avoid a high background of metal ions adsorbed by the membrane surface of the vesicles (*32*). We report here the first results with BLM vesicles (BLMV). Further we also considered what the results tell us about the assay. It had been postulated that the calcein fluorescence quenching assay measured DMT1 activity (*32*). Because it is well established that the G185R mutation diminishes DMT1 activity (*3*, *29*−*31*), a decrease in metal-ion transport in *b*/*b* BBMV would be a critical prediction of the hypothesis that DMT1 was responsible for the activity in this assay. Hence, testing BLMV asks whether DMT1 participates in metal-ion transport at membranes other than those on the apical surface of enterocytes.

We found that activity for transport was below the detection limit in BBMV from *b*/*b* rats. Transport activity was present in +/*b* BLMV preparations but not in *b*/*b* vesicles. We also examined whether antigenic activity associated with DMT1 was still present in the vesicles, relying on isoform specific antibodies. At least four isoforms of DMT1 exist (reviewed by *33*). Polyclonal antibodies (*34*) distinguish the protein forms encoded by DMT1 mRNA containing or lacking an iron-responsive element (IRE); hence we refer to them as +IRE and −IRE. The presence or absence of a translated N-terminal exon 1A, with the alternative exon 1B not translated (*35*), makes exon 1A a unique region for some species of DMT1, so we used an epitope-specific antibody that recognized 1A (*36*). The results show that the various isoforms are still present in vesicles with the +IRE and 1A species, particularly elevated in *b*/*b* BBMV, probably reflecting a response to the severe iron deficiency. Preliminary accounts of some of these results have appeared as abstracts (*37*, *38*).

EXPERIMENTAL PROCEDURES

Materials. $NiCl_2 \cdot 6H_2O$ and $MnCl_2 \cdot 4H_2O$ were from Baker (Phillipsburg, NJ). Triton X-100 and 4-(2-aminoethyl)-benzenesulfonyl fluoride hydrochloride (AEBSF) were from Roche (Mannheim, Germany). Sepharose CL-4B was from Pharmacia (Uppsala, Sweden). Ketamine/Rompun was supplied by the SUNY (Buffalo) Laboratory Animal Facility. All other reagents were from Sigma (St. Louis, MO).

Animals. Belgrade *b*/*b*, +/*b* rats are descendants of the original Belgrade colony backcrossed onto a Fischer 344 background. Most animals in this study are from interbreeding into the Fischer background after the N_8 generation and products of crosses between *b*/*b* males crossed with +/*b* females; thus both +/*b* rats and their *b*/*b* littermates had ∼68.4% Fischer background and ∼31.6% Wistar background. Only *b*/*b* rats are anemic, and are hence paler and smaller than +/*b* rats, which do not show any phenotypical abnormalities. All the rats were fed a normal diet of Purina rat chow supplemented with $FeSO_4$ as described (*13*). Animal procedures were reviewed and approved by the SUNY Institutional Animal Use and Care Committee.

Preparation of BBMV. The protocol for BBMV preparation as described earlier (*32*) for rabbit small intestine was scaled down and adapted to the smaller size of the rat duodenum. Rats were fasted overnight except for access to 5% glucose ad lib to clear the intestine of food. Deep anesthesia was induced by injection of Ketamine/Rompun IM and the small intestine exposed by incision. About 20 cm of rat small intestine (2−2.5 g wet weight) comprising duodenum and upper jejunum were taken, then the rat was immediately sacrificed by cutting the superior aorta. The intestinal tube was flushed with ice cold normal saline and processed directly.

The intestine was briefly rinsed with ice cold NaCl buffer (0.15 M) and cut open for scraping on a glass plate cooled from below with ice. The scraped mucosal cells were collected in 20 mL of ice-cold TME buffer (0.012 M Tris/HCl, pH 7.1, 0.3 M mannitol, 0.005 M EGTA) containing PMSF (1 mM) and antipain (1 μg/mL). While we transferred the suspended enterocytes into a Waring Blender 700 (model 33BL79), we diluted the buffer with 80 mL of deionized distilled H_2O (1:5). The cells were homogenized in the blender twice for 2 min at the highest speed. After the first homogenization, 400 μL of dissolved $MgCl_2$ (2.5 M) were added to reach a final concentration of 10 mM.

The homogenate was kept on ice for 20 min before centrifugation (at 2500 g for 15 min at 4 °C) to sediment cell membranes. These were retained for BLM collection below. The supernatant containing the BBMV was decanted and recentrifuged (at 27 000 g for 30 min at 4 °C). The pellet was resuspended in 6 mL of ice cold Hepes buffer (0.05 M Hepes−NaOH, pH 7.4, 0.1 M NaCl) using a 10-mL Potter-Elvehjem homogenizer at 2000 rpm and centrifuged as before. BBMVs were resuspended in a small amount of Hepes buffer (according to pellet size) containing 300 mM mannitol. Aliquots of 100 μL of BBMV suspension were snap frozen in liquid nitrogen then stored at −70 °C.

Loading of BBMV with Calcein. The fluorescent dye, calcein, was entrapped in the cavity of BBMV by homog-

enization of 0.15 mL suspension of BBMV (2.5−4 mg protein/mL) in Hepes buffer containing the desired concentration of calcein (35 μM) with a Potter-Elvehjem homogenizer at room temperature. External calcein was separated from the calcein-loaded vesicles by gel filtration of the BBMV suspension (0.15 mL) on Sepharose CL-4B (1.5 mL packed in a 2-mL graduated pipet), equilibrated, and run with Hepes buffer. Protease inhibitors were omitted from these steps and in the transport measurements below to minimize the likelihood that the inhibitors would affect transport.

Measurement of Transport of Iron and Other Transition-Metal Ions into BBMV. Because comparison of the transport capacity of BBMV from phenotypically normal +/*b* rats with those from anemic *b*/*b* Belgrade rats was critical, experiments on both types of BBMV were carried out in parallel the same day to guarantee identical conditions for loading of vesicles, buffers and temperature. The experiments were exclusively performed with BBMVs preloaded with 35 μM calcein and incubated routinely with 80 μM of the desired metal ions freshly diluted from 1 mM stock solutions, except for iron, where 50 μM Fe(II)/500 μM AA was used. Start time was the addition of the dissolved metal ions and immediate mixing of the cuvette contents using the pipet tip. At this time zero, recording of the quench curve was also started and followed until equilibration.

Loaded BBMVs were measured on a Perkin-Elmer LS 50B luminescence spectrometer by a continuous fluorescence assay (excitation 490 nm, emission 520 nm) described earlier (*32*). Quenching of the probe calcein monitored transport of divalent transition metal ions across the BBM into the cavity of these vesicles, assay B (*32*). A quenching curve was measured for calibration of ion concentration. For calibration and measurements, a cuvette from Hellma Type 176.751-QS with a path of 3×3 mm^2 was used. Experimental quenching curves were fitted adequately by a Gaussian function. This transport assay responds only to metal ions reaching the lumen of BBMV either bound to the inner membrane surface or free in the cavity. Calcein bound to the external membrane surface and not removed during gel filtration is only detected as a background signal. Kinetic curves were fitted with Mac Curve Fit (Kevin Raner Software, Victoria, Australia) and Excel (Microsoft) by a double-exponential function for kinetic constants. Activation energies (E_a) for Ni^{2+} transport across the BBM were obtained from the slopes of the straight lines derived from points in the Arrhenius plot: slope $= -E_a/R$, where R is the gas constant.

BLM Collection and Aliquoting. The first (BLM) pellet of the BBMV preparation contains all cell membranes except the BBM, which does not precipitate at 10 mM $MgCl_2$. This BLM pellet was resuspended in excess (1:5) diluted TME buffer then otherwise treated and processed like the second pellet containing BBMV as described above. What results is actually a mixture of cell membranes dominated by the BLM of the enterocytes. The exact fraction of membranes from cell organelles and basolateral origin is uncertain. Because results with this preparation may be taken as rough estimates of the state of the BLM, we refer to them as BLM or BLMV for short. As can be seen in the results, however, transport activity of these nominal BLMVs reflects the genotype as does activity patterns of BBMV. The protein content and alkaline phosphatase activity nevertheless reflect the presence of distinct membrane constituents in the BLMV (39).

Analytical Methods. Protein concentrations were determined with a commercial kit (Pierce, Rockford, IL) based on a published method (*40*). Concentrations were always adjusted to match before fluorescence studies. Alkaline phosphatase activities were determined with a commercial kit (Roche, Indianapolis, IN) to evaluate enrichment of BBM and removal of BBM from BLM.

Immunoblots. For segments of the gastrointestinal tract, rats were handled as above except that the entire small intestine was initially collected and rinsed. The proximal fraction was taken to represent the duodenum, the next, to represent the jejunum, and the distal, to represent the ileum. Protein extracts were made by homogenization in PBS containing 1% NP-40, 0.5% deoxycholate, 0.1% sodium dodecyl sulfate (SDS), 10 mM NaF, 1 mM $VOSO_4$, 1 mM PMSF, and protease inhibitor cocktail (Roche, Indianapolis, IN), pH 7.4, then centrifuged for 10 min at 10 000 g and 4 °C. The supernatant was aliquoted and stored at −80 °C until use. Selected amounts of protein from each fraction were subjected to SDS-polyacrylamide gel electrophoresis (PAGE) on a 4−15% gradient acrylamide gel (Bio-Rad, Hercules, CA). Then the proteins were transferred to nitrocellulose membranes by electrophoretic transfer and treated with affinity-purified antibodies specific for the +IRE, −IRE, and 1A isoforms. The first two primary antibodies have been described earlier (*34*); 1A antibody (*36*) was directed against the peptide CELKSYSKSTDPQVST (BioCarta, San Diego, CA). The primary antibodies were detected using monoclonal horseradish peroxidase-conjugated secondary antibody for rabbit IgG (Sigma) with an ECL Kit (Amersham, Piscataway, NJ) and exposed on Biomax imaging films (Kodak, Rochester, NY).

For blots on BBM and BLM, preparations were carried out as described above for BBMV and BLM, but vesicles were not subsequently prepared from the membranes, and the protease inhibitor cocktail was used to minimize proteolysis.

Immunofluorescent Microscopy. For this procedure, rat intestines were prepared as above and then flash frozen in liquid nitrogen. A piece of duodenum was chipped off, exchanged into frozen Tissue Freezing Medium (Triangle Biomedical Sciences, Durham, NC), and sectioned into 10-μm sections on slides using a HM505E microtome by the SUNY at Buffalo Department of Pathology Histology Service. The sections were fixed in methanol at −20 °C for 5 min, washed 3 times in PBS at 4 °C, circled with a liquid blocker Pap pen, blocked with 20% normal goat serum in PBS for 1 h at room temperature, stained with primary antibody (those above) overnight at 4 °C in a humid chamber, rinsed with 2% normal goat serum, 0.1% Triton X-100 in PBS 3 times for 5 min each, stained for 1 h at room temperature with 1/400 goat anti- rabbit IgG conjugated to Alexa568 (Molecular Probes, Eugene, OR), rinsed in PBS 3 times for 5 min, then mounted on coverslips with VectaShield (Vector, Burlingame, CA) and examined in a confocal fluorescent microscope as previously described (*34*).

RESULTS

Capacity of Membrane Transport in b/b and +/b BBMV. Preparations of BBMV from the proximal small intestinal

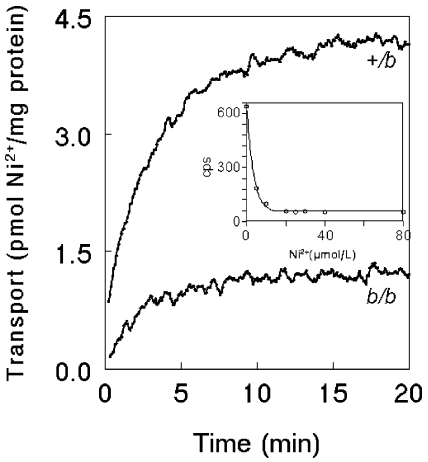

FIGURE 1: Comparison of the transport of divalent metal ions in duodenal BBMV originating from +/*b* and *b*/*b* Belgrade rats. Curves for Ni^{2+} transport are plotted normalized to the protein concentration based on measurements at 25 °C during incubation of BBMV loaded with 35 μM calcein and exposed to 80 μM Ni^{2+} for 20 min with nearly identical concentrations (0.40 +/*b* and 0.38 *b*/*b* mg protein/mL). A large loss in transport capacity is evident for the *b*/*b* curve. Prior to data reduction, the signal for the *b*/*b* BBMV is in the range of 20−25% of that for the +/*b* BBMV, but the signal's properties are like those earlier assigned to calcein located outside of the vesicles (*32*). Moreover the time course of Ni^{2+} transport for the *b*/*b* does not fit an exponential similar to that observed for the +/*b* curve. Therefore transport of Ni^{2+} ions into *b*/*b* vesicles is nearly entirely lost. The inset is a calibration curve of photon counts per second (cps) from calcein as a function of Ni^{2+} concentration. It shows how the Ni^{2+} transport was calculated; the curve was fitted to the experimental calcein quenching as in the previous study (*32*). The useful response range starts at zero and runs up to 25 μmol/L.

tubes of *b*/*b* and (as control) +/*b* rats did not reveal any morphological changes and did not present any complications compared to the normal rabbit preparation (*32*). Experiments with BBMV of +/*b* and *b*/*b* Belgrade rats yielded kinetic data for evaluating transport capacity for Ni^{2+} (Figure 1). Transport was clearly present in +/*b* BBMV but essentially absent with *b*/*b* BBMV. Only quenching of calcein bound to the outer vesicle surface was detected in BBMV of *b*/*b* rat origin. This absence implies that the missense mutation of a single amino acid (G185R) in DMT1 is responsible for an essentially complete loss of the transporter function and verifies that DMT1 transports Ni^{2+}. Conversely, the loss of activity with the G185R mutation verifies that the activity assayed is due to the transporter as predicted (*32*) and that the assay developed on rabbit intestinal preparations adapts to rats.

Transport of Transition-Metal Ions across the BBM. One aim of this study was to confirm that DMT1 is the transporter for transition metals in the BBM. Therefore several divalent transition-metal ions were tested for transport activity in rat BBMV (Figure 2). The measurement curves in +/*b* BBMV confirmed the transport of Mn^{2+}, Fe^{2+}, and Ni^{2+} into the vesicle cavity with similar time courses to those for rabbit BBMV. The essentially complete failure of transport in *b*/*b* BBMV demonstrates that transport activity in +/*b* rat vesicles (here) and rabbit BBMV (*32*) is due to DMT1. Figure 2 also illustrates an overshoot in the loss of fluorescence intensity by calcein contained in the vesicle cavity, particularly associated with Mn^{2+} and Fe^{2+} transport at higher temperatures. This overshoot occurs very likely because of acidification of the vesicle cavity, apparently due to proton cotransport with the initial quenching reversed over time presumably by proton equilibration to re-establish vesicle pH. This situation is consistent with proton-coupled transport occurring in the +/*b*. The proton transport must occur in a brief time frame to cause the overshoot and subsequent decrease in quenching while the vesicle pH dynamically re-equilibrates. With Ni^{2+}, the overshoot was absent, suggesting that the slower speed of transport allows time enough for pH re-equilibration. This behavior was similar to results where Ni^{2+} exhibited no overshoot while other divalent metal ions did show overshoot in rabbit BBMV (*32*). Activity was absent for each tested transition-metal ion (Mn^{2+} in Figure 2, Ni^{2+} in Figure 1, and Fe^{2+} not shown) in BBMV from *b*/*b* rats.

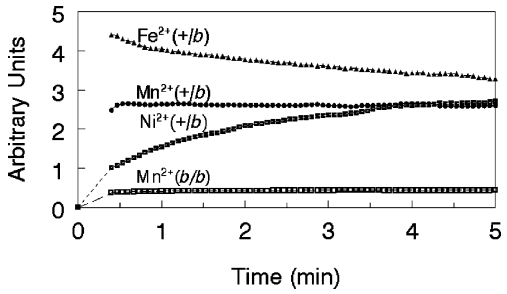

FIGURE 2: Time course for transport of selected transition-metal ions across the membrane of calcein-loaded BBMV. Loss of fluorescence intensity is plotted in arbitrary units against time. The transport experiments are for Fe^{2+}, Mn^{2+}, and Ni^{2+} with +/*b* BBMV and Mn^{2+} with *b*/*b* BBMV. The experiments were carried out at 30 °C. Fast transport of Fe^{2+} and Mn^{2+} resulted in an overshoot in loss of fluorescence intensity for +/*b* BBMV with the extent of the overshoot being very modest for Mn^{2+}. Transport of Ni^{2+} by +/*b* BBMV is slower so no overshoot occurs. The *b*/*b* BBMV also lack the overshoot and the time course with Mn^{2+} resembles the results with Ni^{2+} in Figure 1, again consistent with loss of transition metal transport by the vesicles.

The quenching standard curve (inset to Figure 1) was used to calibrate a series of Ni^{2+} transport assays to obtain information about kinetic constants (Figure 3). The decay in fluorescence was converted into time-dependent (increasing) ion concentration within the vesicle cavity. These curves were fitted by a double-exponential function from which pseudo-first-order rate constants (k_1) were derived as done previously (*32*). The +/*b* data (A) yielded k_1 values and half times that varied with temperature as expected for a catalyzed transport process; while the *b*/*b* kinetic curves (B) are consistent with relatively rapid quenching of external calcein. The average value of the second phase's pseudo-first-order rate constant for Ni^{2+} at 30 °C (Figure 2 and replicates) was $k_1 = 0.66 \pm 0.14$ min^{-1} ($t_{1/2} = 1.04$ min, $n = 5$). This second slower process represents the transport of metal ions across the BBM. The first phase was characterized by a pseudo-first-order rate constant, $k_1 = 3.22 \pm 0.74$ min^{-1} ($t_{1/2} = 12.9$ s, $n = 7$), representing rapid quenching of calcein bound outside of the vesicles. This value should be and is in the same range as published before for rabbit experiments (*32*). It is also similar to the constant calculated for the *b*/*b* transport curves and supports the argument that this process is the only one that occurs with *b*/*b* vesicles. Data modeling (not shown) using the two exponential functions above and adding different fractions of the slower process to the faster one indicate that we might visually detect 1% residual activity with just exponential processes. The undulations and

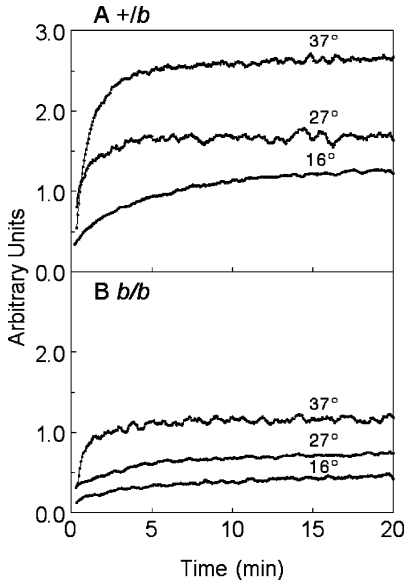

FIGURE 3: Typical experimental curves used to fit pseudo-first-order rate constants, k_1. Ni^{2+} transport across the membrane of BBMV was measured as in Figure 1 with heterozygous +/*b* (A) and homozygous *b*/*b* (B) samples. Calcein-loaded BBMV again were mixed with 80 μM Ni^{2+} at time zero and incubated. Transport was measured at 37, 27, and 16 °C. A double-exponential function was fitted to these curves as done for rabbit BBMV previously (*32*); pseudo-first-order rate constants (k_1) were derived from the fits (Table 1).

Table 1: Temperature-Dependence of Pseudo-First-Order Rate Constants k_1 for Ni^{2+} Transport Across Rat BBMs[a]

temperature (°C)	k_1 (min^{-1})	$t_{1/2}$ (min)
16	0.31 ± 0.10	2.2
18.5	0.34 ± 0.02	2.1
22	0.37 ± 0.14	1.8
26	0.40 ± 0.16	1.7
27.5	0.67 ± 0.23	1.0
30	0.66 ± 0.14	1.0
32	0.86 ± 0.12	0.8
35.5	0.98 ± 0.14	0.7

[a] Curves for Ni^{2+} transport such as those in Figure 3 were fitted to a double-exponential function (*32*); pseudo-first-order rate constants (k_1) and half times, $t_{1/2}$, were derived from this fit.

other noise visible in the figure, however, reduce the sensitivity. Probably 2% residual activity could be detected if present in *b*/*b* data, but it is doubtful that a lesser level would be detected.

Experiments with Ni^{2+}, the metal ion having the slowest transport rate, resulted in about the same kinetic constants as previously found for rabbit tissue (Table 1). The temperature dependency of the kinetics of Ni^{2+} transport into +/*b* BBMV was measured in the range from 16 to 35 °C. Although the confidence intervals were larger for rat BBM, the kinetic constants for transport resembled those for the rabbit BBM (*32*). The composition of rat BBM compared to rabbit BBM might therefore have little effect on the transition temperature of the membrane. Plotting these and additional k_1 values yielded an Arrhenius plot that could be fitted as in the rabbit (*32*) by two straight lines with an intersection at 23.5 ± 1 °C (Figure 4). The slopes of these straight lines indicate comparable activation energies (E_a) to those for the identical transport process in rabbit BBMV (*32*). The E_a for the temperature range between 16 and 28.5 °C corresponded to the earlier determined E_a = 21.2 kJ/mol (5.09 kcal/mol), and the estimate was again in the same range as for results with rabbit BBMV above 27 °C with E_a = 62.0 kJ/mol (14.8 kcal/mol).

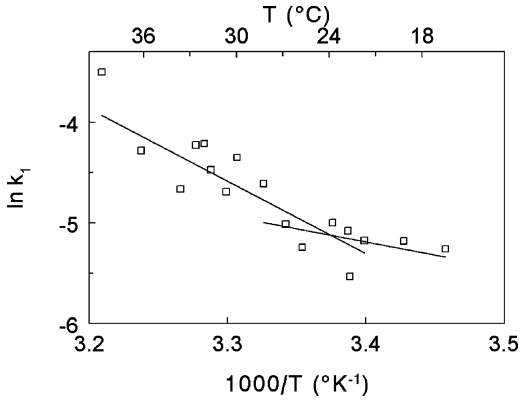

FIGURE 4: An Arrhenius plot with pseudo-first-order rate constants k_1 from 32 experimental curves for 17 series ranging from 16 to 38.5 °C graphed as ln k_1 versus 1000/*T*. The data points of the Arrhenius plot were fitted to two straight lines in accordance with previous experiments on rabbit BBMV (*32*). These lines intersected at 23.5 ± 1 °C here in contrast to 24 °C in the rabbit data. Below 23.5 °C, the straight line (lower right) in the graph defined by $y = 3.52 - 2561x$ ($R^2 = 0.957$) yielded an activation energy, E_a = 21.2 kJ/mol (5.09 kcal/mol). At temperatures above 23.5 °C, the line (upper left) fit to this data set by $y = 23.0 - 8359x$ ($R^2 = 0.757$; E_a = 69.4 kJ/mol = 16.6 kcal/mol) differed only slightly from the line given by $y = 20.0 - 7463x$ ($R^2 = 0.907$; E_a = 62.0 kJ/mol = 14.8 kcal/mol) from the previous rabbit experiments with a slightly higher E_a for rat BBMV.

Transport of Transition-Metal Ions across the BLM. Enterocytes are polarized cells. Their polarity results in two functionally specialized membranes: The apical and basolateral membranes. The flow of nutrients through the apical BBM is exclusively directed into the cell. The BLM must regulate the flow of nutrients into the circulation, but also this membrane needs reverse functions to access nutrients from the body as needed. Therefore DMT1 might be found not only in the apical membrane but also in endocytic vesicles originating from the basolateral membrane. To address this question experimentally, nominal BLMs were prepared and calcein loaded as described for BBMV to measure transport activity.

Although some BLMV were lost during gel filtration on the first layer of the gel possibly due to their size, the remaining vesicles were similar to BBMV in their transport properties as measured by fluorescence quenching. Transport activity behaved as expected for DMT1 and +/*b* BLMV were active while *b*/*b* BLMV were inactive just as was found in BBMV (Figure 5). Even though the basolateral fraction might contain contaminating organelle membranes, +/*b* vesicles contained a transport system operating similar to DMT1. For the *b*/*b* vesicles, no transport activity could be detected, so alternative transport systems do not work under the assay conditions. Over a smaller temperature series, the derived pseudo-first-order rate constants of the putative basolateral form of the transporter were indistinguishable from those of BBMV-derived transporter. The extent of Ni^{2+} transport also did not differ for the two vesicle preparations. Even an overshoot in loss of fluorescence intensity suggesting proton cotransport and re-equilibration was observed for Fe^{2+} and Mn^{2+} transport. Our results indicate that DMT1, although

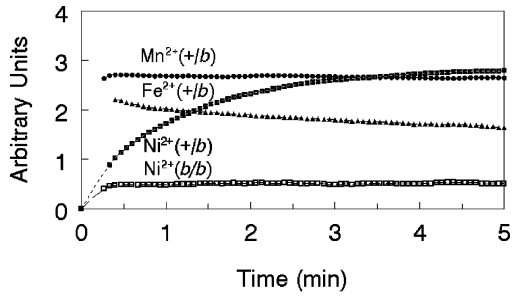

FIGURE 5: Transport of selected transition-metal ions across the membrane of calcein-loaded BLMV. The transport experiments are for Mn^{2+}, Fe^{2+}, and Ni^{2+} with +/*b* BLMV and Ni^{2+} with *b*/*b* BLMV. The experiments were carried out at 30 °C. Fast transport of Mn^{2+} and Fe^{2+} resulted in an overshoot in the curve for +/*b* BLMV with the extent of the overshoot being very modest for Mn^{2+}. Transport of Ni^{2+} by +/*b* BLMV is slower, so no overshoot occurs. The *b*/*b* BLMV also lack the overshoot and exhibit a time course that resembles *b*/*b* results with Ni^{2+} in Figure 1 and Mn^{2+} in Figure 2, again consistent with loss of transition-metal transport by the vesicles. The transport properties of +/*b* BLMV are very similar to those of +/*b* BBMV (Figures 1 and 2), while the transport properties of *b*/*b* BLMV are indistinguishable from those of *b*/*b* BBMV (Figures 1 and 2).

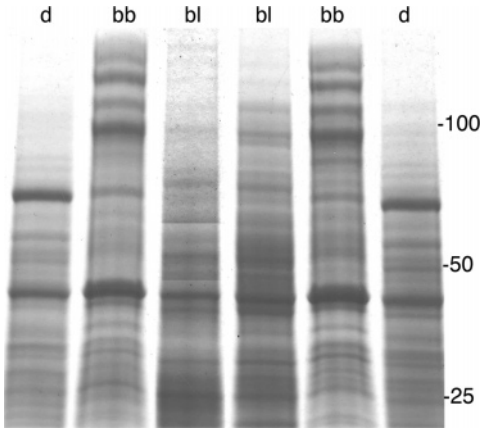

FIGURE 6: Proteins in duodenal extracts, BBM and BLM. Fifteen μg of protein from duodenal extracts, BBM, and BLM were analyzed by SDS-PAGE as described for immunoblots but stained with Coomassie Blue. The positions of marker proteins of 25, 50, and 100 kD are indicated. The 3 lanes on the left were from a +/*b* rat; the 3 lanes on the right were from a *b*/*b* rat. The sources are designated d for duodenal extracts, bb for BBM, and bl for BLM. Each fraction has a distinct protein content, but +/*b* or *b*/*b* origin did not affect the protein pattern.

enriched on the BBM, is also present on other membranes of duodenal extracts.

Because this conclusion is dependent on the BBMVs and BLMVs being distinct preparations with BLMV depleted of BBMV, we examined the preparations by SDS-PAGE. Proteins at ~115 and 130 kD were unique markers for BBMV and absent from BLMV after staining with Coomassie blue (Figure 6). A protein at ~75 kD was a marker for BLM, and additional proteins were enriched in BBM or BLM. Duodenal extracts, BBM, and BLM were also assayed (Table 2) for alkaline phosphatase activity, another BBM marker (*39*). BBMs were 15-fold enriched in alkaline phosphatase compared to the duodenal extracts, whereas BLM and duodenal extracts had similar levels. We also tested some of their properties by immunoblotting below.

The data in Figures 1, 2, and 5 show that DMT1 transport activity is deficient in BBMVs and BLMVs of *b*/*b* origin.

Table 2: Alkaline Phosphatase Activity in Membrane Fractions

fraction	activity[a]
duodenal extract	19 ± 10[b]
BLM	40 ± 24
BBM	291 ± 94

[a] UI/μg protein as mean ± SD for $n = 5$. [b] Alkaline phosphatase activities in *b*/*b* and +/*b* preparations were not significantly different so long as we compared only BBM or only BLM or only duodenal extracts so data were combined across genotypes for BBM, for BLM, and for duodenal extracts. Oneway ANOVA for duodenal/BBM gives $P = 0.027$, ANOVA for BLM/BBM gives $P = 0.038$, whereas for duodenal/BLM it gives $P = 0.6$.

The G185R mutation could inactivate the transport activity or cause improper localization, or there could be a combination of effects. The possibility that DMT1 is no longer targeted properly has been raised by studies in the *mk*/*mk* mouse where the identical G185R mutation (*2*) has occurred. The transporter may be targeted incorrectly in the duodenum (*42*) of the *mk*/*mk* mouse. Arguments that it is similarly incorrectly located in *mk*/*mk* reticulocytes (*43*) and kidney (*44*) have also been published. We therefore tested for whether DMT1 protein was missing from or diminished in BBMV and BLMV by immunoblotting immediately below. Further below, we also examined localization of DMT1 by immunofluorescent confocal microscopy.

Immunoblotting to Detect DMT1 Isoforms. Previous evidence (*1*, *4*) suggests that the +IRE isoforms of DMT1 are enriched in the duodenum and increase in response to iron deficiency. This evidence reflects the cloning of the +IRE form from that tissue (*1*) and detection of DMT1 using antibody to the common N-terminal region which therefore ought to react with all isoforms (*4*), combined with an inability to detect the −IRE form with a putatively specific antibody. We first investigated the distribution of epitopes in the intestine (Figure 7) with +IRE specific antibody (*34*). Increased immunoreactivity after transient ectopic expression of DNA expressing this isoform but not an untransfected control nor transfections expressing other isoforms (panel A) verified the specificity of the antibody. This specificity was confirmed for intestinal tissue by inhibition of immunoreactivity when the antigenic peptide was present (panel B) and absence of bands (not shown) when the primary antibody was omitted. The +IRE antibody therefore has the specificity required to address whether +IRE DMT1 localizes appropriately in *b*/*b* duodenal fractions.

A 70-kD species was the main species of +IRE DMT1 present in the small intestine (Figure 7, panel C), although other species were also detected. Because the relative quantity of the various isoforms of DMT1 is more germane to the critical issues than the apparent size of the species observed, results on the proportions of +IRE DMT1 are presented here. The critical issues are whether normal transport activity is lost after the G185R mutation due to inactivation of the transport activity, improper targeting, or gross instability of the mutated transporter and whether BBMV and BLMV represent distinct membrane fractions. Reported sizes of DMT1 isoforms vary depending on the source, antibody, and laboratory (*36*) and deserve, but have not yet received, a systematic exchange among laboratories studying them. The data in this paper do illustrate that some of the variation reflects the concentration of DMT1 present.

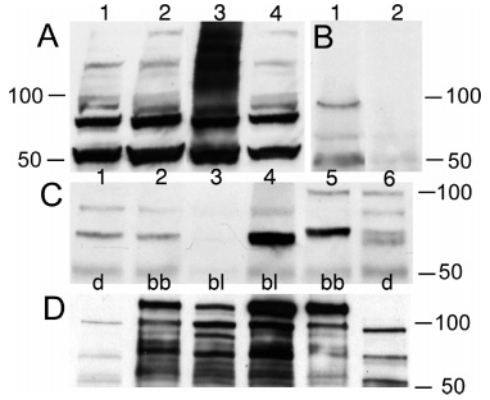

FIGURE 7: Immunoblotting of the +IRE isoforms of DMT1. All panels depict reaction with antibody specific for the +IRE isoforms of DMT1. The positions of marker proteins of 50 and 100 kD are indicated for all panels. While each lane contains 35 μg of protein in panels A−C, each lane contains 15 μg in panel D. (A) Comparison of HEK293 cells transfected with constructs transiently expressing various rat DMT1 isoforms (*36*) or untransfected cells, including 2/-IRE DMT1 (lane 1), 1A/-IRE DMT1 (lane 2), 1A/+IRE DMT1 (lane 3), or untransfected cells (lane 4). Multiple endogenous +IRE species are present in lane 4 with the major bands at ∼50 and 70 kD. Both bands increase in lane 3, and a prominent smear of additional immunoreactivity is visible at higher molecular weights. As expected, this increase does not occur when the transfecting DNA expressed an isoform of DMT1 that lacks the +IRE epitope (lanes 1 and 2). (B) Blocking of gastrointestinal +IRE DMT1 detection. Duodenal immunoreactivity (∼50, 70, and 95 kD: lane 1) is blocked by immunizing peptide (1 μg/mL: lane 2). (C) Distribution of the +IRE species in rat small intestine. Lanes 1−3 are from a +/*b* rat; lanes 4−6 are from a *b*/*b* rat. Lanes 1 and 4 are from the duodenum, lanes 2 and 5 are from the jejunum, and lanes 3 and 6 are from the ileum. Immunoreactivity is present (∼50, 70, 90, and 99 kD, depending on lane), exhibits a decreasing trend along the length of the small intestine, and is relatively higher for corresponding segments of *b*/*b* small intestine compared to +/*b*. These results are representative of 5 series of analyses with the lane to lane variation occurring in each run. D. Comparison of duodenal extract, BBM, and BLM for content of the +IRE isoform of DMT1. Extracts from +/*b* (lanes 1−3) contain less +IRE DMT1 than *b*/*b* extracts (lane 4−6); duodenal content (lanes 1 and 6-d) is substantially less than that of BBM (lanes 2 and 5-bb) or of BLM (lanes 3 and 4-bl). The +IRE isoforms of DMT1 are considerably enriched in the BBM and BLM with the same sizes present as in the duodenum plus an additional band at ∼115 kD. The most likely explanation for the 115-kD band is that its presence is dependent on the concentration of DMT1 present. These results are representative of 3 series of analyses with the lane to lane variation occurring in each run.

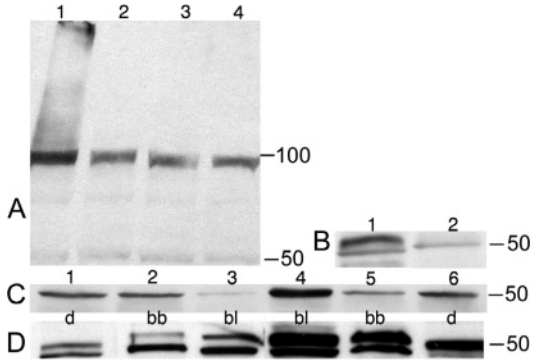

FIGURE 8: Immunoblotting of the −IRE isoforms of DMT1. All panels depict reaction with antibodies specific for the −IRE isoforms of DMT1. The positions of marker proteins of 50 and 100 kD are indicated for panel A; only 50-kD marker proteins are indicated for B−D. While each lane contains 35 μg of protein in panels A−C, each lane contains 15 μg in panel D. (A) Comparison of HEK293 cells transfected (*36*) with the 1A/-IRE form of rat DMT1 (lane 1) or with the 2/+IRE form (lane 2) or with the 1A/+IRE form (lane 3) or not transfected (lane 4). Two endogenous −IRE species are present in lanes 2, 3, and 4 with the major band just below ∼100 kD and the minor one at ∼50 kD. The major band increases in lane 1, and additional immunoreactivity is visible above 200 kD. (B) Gastrointestinal −IRE DMT1 detection is specific; duodenal immunoreactivity is visible at ∼50 and 55 (lane 1), and 100 kD (not shown) is blocked by immunizing peptide (1 μg/mL, lane 2). (C) Distribution of the −IRE species in rat small intestine. Lanes 1−3 are from a +/*b* rat; lanes 4−6 are from a *b*/*b* rat. Lanes 1 and 4 are from the duodenum, lanes 2 and 5 are from the jejunum, and lanes 3 and 6 are from the ileum. The main −IRE species is ∼50 kD; an additional species at ∼55 kD and a minor species at or slightly larger than ∼100 kD were inconsistently visible in some lanes but none of the ones shown. These results are representative of 5 series of analyses with some lane to lane variation occurring in each run. The tendency for the *b*/*b* duodenum to have a minor elevation of −IRE DMT1 is well represented by this figure; differences in levels between jejunum and ileum were inconsistent. (D) Comparison of duodenal extract, BBM, and BLM for content of the −IRE isoform of DMT1. Extracts from +/*b* (lanes 1−3) contain less −IRE DMT1 than *b*/*b* extracts (lane 4−6); duodenal content (lanes 1 and 6-d) is substantially less than that of BBM (lanes 2 and 5-bb) or of BLM (lanes 3 and 4-bl). The −IRE isoforms of DMT1 are considerably enriched in the BBM and BLM with a ∼50-kD species present as in the duodenum plus an additional band at ∼55 kD. This band is also present in +/*b* duodenum in this panel. These results are representative of 3 series of analyses with some lane to lane variation occurring in each run.

The +IRE species was more prevalent in the duodenum than the jejunum of +/*b* rats and even more decreased in the ileum. It was obviously elevated in the duodenum and jejunum of *b*/*b* rats and even the ileum of *b*/*b* had about as much as the duodenum or jejunum of +/*b* rats. These differences match the expectation for severe chronic iron deficiency. Thus the absence of transport activity occurs despite increased levels of protein. We tested the possibility that this protein is improperly targeted as observed for the duodenum of *mk*/*mk* mice (*42*) by analyzing BBM and BLM for immunoreactivity. Immunoreactivity was elevated in *b*/*b* BBM and BLM just as in +/*b* BBM and BLM; this increase is associated with the presence of additional protein bands for both genotypes (Figure 7, panel D). Interestingly, there appears to be a higher density of the +IRE isoforms in the BBM of +/*b* rats than in their BLM although both are enriched compared to duodenal extracts. The enrichment in the +IRE isoforms was even more noticeable in *b*/*b* BLM than in *b*/*b* BBM, suggesting that the response to iron deficiency is not limited to apical membranes and may even be greater in other cellular membranes. These observations indicate that lack of G185R transport activity is due to the mutation inactivating transport rather than causing grossly improper localization of the transporter although the higher enrichment of +IRE DMT1 in *b*/*b* BLM compared to BBM could indicate a degree of dislocalization. The extent of improper localization, however, does not seem to be as great as that reported for *mk*/*mk* DMT1 nor are the results on the other isoforms in *b*/*b* enterocytes and on immunofluorescent localization (below) consistent with a large degree of dislocalization.

We also investigated the −IRE antibody (Figure 8) for better ability to detect this species of DMT1 than the antibody in the previous report (*4*). Panel A indicates that it has the desired specificity, detecting transient ectopic expression of −IRE species but not that of two +IRE species. Untrans-

fected cells (lane 4) exhibited the same patterns as lanes 2 and 3, verifying that the bands detected represent endogenous −IRE isoforms. The immunizing peptide specifically blocked immunostaining to confirm this specificity (panel B) as did absence of any staining after omission of the primary antibody (not shown).

The −IRE isoforms are mainly represented in a 50-kD species in the small intestine (Figure 8, panel C) that responds to the chronic iron deficiency of *b*/*b* rats with a modest enrichment in the duodenum. This small elevation in immunoreactivity appears due to a larger increase in the −IRE isoforms in *b*/*b* BLM than in BBM, but both the ∼50- and 55-kD species (panel D) are enriched in the vesicles from both genotypes. The modest increase in −IRE DMT1 in both vesicle fractions from *b*/*b* enterocytes is consistent with a loss of activity for the transporter rather than improper localization.

Polyclonal antibody directed against the rat 1A isoforms, first identified by Hubert and Hentze (*35*), also appears to have the requisite specificity (Figure 9) as detected by blots for regulated expression of a DNA construct (panel A) where high molecular weight forms are overexpressed and an ∼90-kD form increases. Blocking of the reaction by the immunizing peptide confirmed this specificity (compare panel C to B) for species at ∼37, 50, and 90 kD as did omission of the primary antibody (not shown), but these small intestinal samples do have a weak nonspecific band at ∼70 kD.

The response to chronic iron deficiency of the 1A isoforms (Figure 9, panels B and D) is closer to the higher response of +IRE isoforms than the lower one for the −IRE species. Although illustrative of variation in the yields of the ∼37- and ∼50-kD species, panel D clearly shows that BBM and BLM are highly enriched in the 1A DMT1 species with *b*/*b* vesicles having a higher density reflecting the chronic iron deficiency. The data confirm up regulation of this isoform during chronic iron deficiency and support the argument that BBM and BLM contain a higher density of this species than is present in the duodenal extract. The results do not indicate a failure to localize properly, although it is again noticeable that enrichment in *b*/*b* BLM is very high.

Immunofluorescent Localization of DMT1 Isoforms in Duodenal Sections. The localization of DMT1 species in enterocytes was also examined by microscopy after immunofluorescent staining (Figure 10). The results are generally consistent with those outlined above for immunoblotting. Each antibody revealed similar localizations in +/*b* and *b*/*b* sections, although there was stronger staining of the *b*/*b* preparations with +IRE and 1A antibodies, probably reflecting the iron-deficient status of the homozygous mutant rats. All three antibodies stained apical membrane, consistent with western analysis of BBMV. The antibodies did differ in the degree to which they stained basal and lateral membranes (with the +IRE antibody staining both, the −IRE staining lateral membranes poorly if at all, and the 1A antibody staining neither basal nor lateral membranes very well) and in whether they stained intravillarly (and in the intravillar pattern when the 1A and −IRE antibody stained there). Most prior studies have used an antibody directed either against an epitope common to known isoforms of DMT1 or against the +IRE isoform and have missed the distinct isoform specific localizations illustrated here.

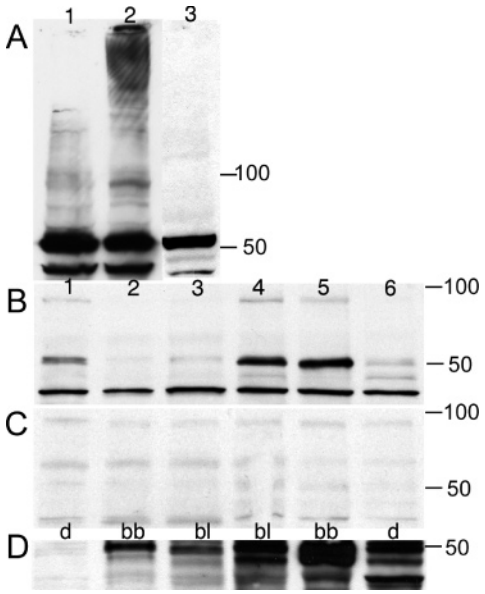

FIGURE 9: Immunoblotting of the 1A isoforms of DMT1. All panels depict reaction with antibody specific for the 1A isoforms of DMT1. The positions of marker proteins of 50 and 100 kD are indicated for A, B, and C; only 50-kD marker proteins are indicated for D. While each lane contains 35 μg of protein in panels A−C, each lane contains 15 μg in panel D. (A) Comparison of HEK293-F cells containing a construct that can express the 1A/+IRE form of rat DMT1 from a tetracycline regulated promoter in the absence of induction by doxycycline (lane 1) or in the presence of doxycyline (lane 2) or containing the empty vector (lane 3). Uninduced expression (already elevated above endogenous expression visible in lane 3) leads to 1A species present in lane 1 with the major bands at ∼50 and 37 kD; induced expression leads to a strong smear of immunoreactivity near 200 kD and an increase in a distinct band at ∼90 kD. (B) Distribution of the 1A species in rat small intestine. Lanes 1−3 are from a +/*b* rat; lanes 4−6 are from a *b*/*b* rat. Lanes 1 and 4 are from the duodenum, lanes 2 and 5 are from the jejunum, and lanes 3 and 6 are from the ileum. A major ∼37-kD 1A species is present in all lanes at essentially the same concentration; a major ∼50-kD species is present in lanes 1, 4, and 5; the ∼50-kD species is a minor band in the remaining lanes. A minor band at ∼90 kD is also present in lanes 1, 4, and 5. The increased content of the ∼50-kD species in the *b*/*b* duodenum and jejunum is probably a response to the iron deficiency in the Belgrade rat; a similar increase in levels of a minor ∼90-kD species in the *b*/*b* duodenum and jejunum might also represent such a response. These results are representative of 5 series of analyses with some lane to lane variation occurring in each run. (C) Gastrointestinal 1A DMT1 detection is specific; immunoreactivity for all of the bands noted in panel B is blocked by immunizing peptide (1 μg/mL). The minor band at ∼70 kD was not blocked and might be nonspecific. D. Comparison of duodenal extract, BBM, and BLM for content of the 1A isoform of DMT1. Extracts from +/*b* (lanes 1−3) contain less 1A DMT1 than *b*/*b* extracts (lane 4−6); duodenal content (lanes 1 and 6-d) is substantially less than that of BBM (lanes 2 and 5-bb) or of BLM (lanes 3 and 4-bl). The major 1A isoform of DMT1 is a ∼50-kD species with a ∼37-kD species also present and another minor species detected when levels are very high. These results are representative of 3 series of analyses with some lane to lane variation occurring in each run.

DISCUSSION

Metal Ion Transport Activity and the G185R Mutation. The data in the present study directly link DMT1 and the protein activity that accounts for transport of transition-metal ions. This activity is responsible for nonreceptor-mediated uptake into BBMV and transport into BLMV. The G185R mutation leads to complete disruption of transport activity of the integral membrane protein in *b*/*b* BBMV and BLMV.

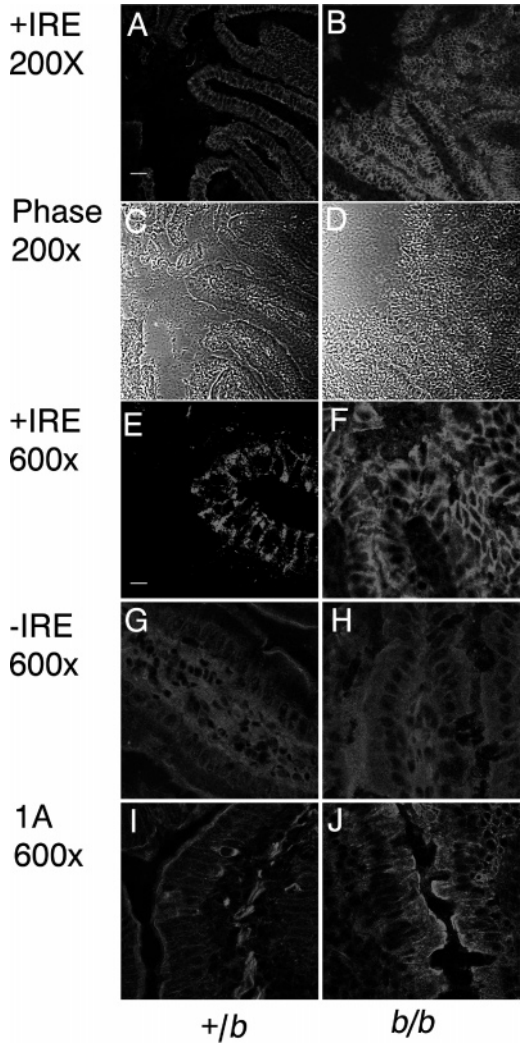

FIGURE 10: Localization of DMT1 isoforms in duodenal sections by immunofluorescent detection in confocal microscopy. Duodenal sections from +/*b* (Panels A, C, E, G, and I) and *b*/*b* (Panels B, D, F, H, and J) were examined by fluorescent detection with a 20× objective (A and B) or a 60× objective (E−J) or phase and a 20× objective (C and D). Bar = 30 μm for A−D; Bar = 10 μm for E−J. The settings were identical for pairwise comparisons (A−B, C−D, etc), but different antibodies or different objectives necessarily required changes in the settings. The +IRE staining is present in +/*b* apical and basolateral membranes (A and E) but absent from much of the enterocytes' cytosol; +IRE staining is considerably elevated in the same membranes of *b*/*b* enterocytes (B and F). Phase images reveal that the microscopic morphology of the *b*/*b* duodenum is similar to that of the normal +/*b* control (C and D). Staining of −IRE epitopes is less marked and occurs to about the same degree in apical and basal membranes of both +/*b* and *b*/*b* enterocytes (G and H); this staining also appears in the intravillar space. 1A staining is primarily present on the apical membrane of +/*b* enterocytes (I) but is faintly visible on other membranes and occurs strongly in the intravillar space in a feathery pattern; while the same pattern is visible in the *b*/*b* section, the apical staining is considerably stronger and has spread punctately into the enterocyte below the BBM. Controls where primary antibody was omitted had no detectable fluorescence and those where reaction of the primary antibody was first blocked with 1 μg/mL of the immunizing peptide exhibited little or no fluorescence (not shown).

The Belgrade rat manifests a well-characterized, microcytic, hypochromic anemia (*7*−*15*). A similar anemia occurs in the *mk* mouse (*17*−*19*). Remarkably, the anemia in both models is caused by identical G185R mutations in the same transporter (*2*,*3*). It is still not clear why exactly this mutation is tolerated in such an essential transport system, but the mutant rodents' survival implies that alternative transport activity might exist or the G185R mutation might be leaky (*45*). No such remaining or leaky transport activity was detected in our model system, neither with BBMV (Figures 1, 2, and 3A) nor with BLMV (Figure 5). Although the fluorescence assay employing calcein-loaded vesicles should have been ideal for detecting passive membrane transport, no such transport was apparent. This absence means that the metal ion transport is not present or below a detection limit of ∼2% imposed by the external membrane-associated calcein, but it is unclear if proton transport is similarly affected under the experimental conditions used.

The data in the present paper indicate that the homozygote for this G185R mutation should lose transport activity of DMT1 in the duodenum. The remaining quenching of about 20−25% takes place mainly during mixing of the samples (Figure 3B). Other than a tiny amount of activity that could be masked by this quenching, the calcein-loaded vesicles should be sensitive to small amounts of metal ions entering the vesicle cavity and should be able to detect even low amounts of ions migrating through the membrane as can be rationalized by the quenching curve (Figure 1 inset). In addition, a signal should be eventually seen when the concentrations outside and inside of the vesicles come into a dynamic equilibrium, but this is not the case. Lack of activity in *b*/*b* BBMV also permits a direct assessment of the stability of the BBM exposed to external metal ions. In previous experiments, negatively charged large unilamellar vesicles with artificial membranes from egg phosphatidylcholine and egg phosphatidic acid (molar ratio = 1:1) retained their integrity in the presence of up to 180 μM Ni^{2+} (*32*). BBMVs should be more stable because of their membrane composition. The apparent total loss in transition-metal ion transport capacity should be compared to data from other groups. Iron incorporation from Tf into Belgrade rat reticulocytes was decreased to ∼20% of normal (*5*, *41*); the same residual as for non-Tf-dependent uptake (*15*). In *mk*/*mk* reticulocytes, however, ∼50% of iron incorporation is retained (*19*, *43*). The apparent retention of flux through the Tf cycle and the implication that there is residual GI iron transport may account for the two mutants' survival and imply that alternative pathways or leakiness exists in vivo (*45*). Ectopic assays (*3*) showed the mutant rat R185 construct had ∼1% as much activity as the wild-type G185 construct while mouse constructs yielded even less residual activity (*29*). Similar assays on Mn transport (*31*) also detected very little residual activity in the *b* mutant; the human R185 construct, however, retained ∼15% activity (*30*). While this Ms was undergoing review, yet another paper on the issue of retention of transport activity appeared (*46*) comparing ectopic expression of wild type and *mk* constructs for Fe and Co uptake. The authors detect substantial residual activity in the G185R mutant, but the mutant is also unstable, less well glycosylated, and partly incorrectly targeted in their hands. Clearly the conclusion on residual activity depends on the nature of the assay.

Kinetics of Fe^{2+} and Mn^{2+} transport (Figure 2) could not be evaluated the same way as for Ni^{2+}. Transport of these metal ions was much more rapid so that cotransport of a proton [H^+] into the cavity of BBMV (*32*) probably led to proton re-equilibration at higher temperatures. The metal ion

and proton flux occurred simultaneously probably because vesicles did not have sufficient time after the cotransport to restore their pH. This coincidence obstructed calculation of vesicle metal ion concentrations, a conversion essential for fitting the data. There is no doubt, however, that metal ions reached the cavity of BBMV from +/*b* rat tissue, whereas no such effects were measured with *b*/*b* BBMV. Although metal ions were not released from the vesicle cavity after transport, the outward-directed proton gradient probably reached a maximum then decreased just before the vesicle achieved a dynamic equilibrium state for the metal ions. At lower temperatures, evidence for pH change could not be detected. Also Fe^{2+} had to be stabilized in a divalent state by AA, another factor that also prevented calculation of exact vesicle Fe^{2+} concentrations.

Metal Ion Specificity. DMT1's substrate specificity for divalent metal ions previously appeared broad (*1*). There are recent reviews (*33*, *47*) on the metal ions that might be transported. Evidence at the time of the reviews supported the three ions above, but Zn^{2+} transport is controversial. The calcein-based assay with BBMV is an excellent way to verify the metal ion specificity provided that the metal ion actually quenches calcein fluorescence. Zn^{2+} did not quench (*32*), but did evoke a rapid proton flux, illustrating a challenge for interpretation of data. Cd^{2+} (*48*), Pb^{2+} (*49*), and Cu^{2+} or Cu^{1+} (*50*) are other metals that might be tested. In addition it is uncertain whether alternative transport systems for other metal ions might also be present in the BBM. The CTR1 family for copper (*51*) and the ZTL1 transporter family for zinc (*52*) have already been characterized in other systems. Clearly investigation of transport of these metal ions by BBMV deserves to be the subject of further investigation. These investigations should test how such independent transporters can be identified in the BBM and whether they are able to replace the function lost in *b*/*b* DMT1 for the specific metal ion.

Targeting of DMT1 after the G185R Mutation. Residual transport activity in *b*/*b* vesicles was undetectable. Possibly this absence is due to inactivity of the transporter, but it can also be due to improper localization. The transporter is apparently targeted incorrectly after the mutation G185R in three tissues in the *mk/mk* mouse: the duodenum (*42*), the reticulocyte (*43*), and the kidney (*44*). On the other hand, with the identical mutation in a modestly different DMT1 framework in *b*/*b* rats, immunohistochemical staining for DMT1 on the BBM of enterocytes resembles the pattern seen in iron deficiency (*53*) with little evidence for improper localization. The targeting possibility is further complicated in the duodenum by data that show that DMT1 leaves the BBM toward more internal membranes in two situations: In rat duodenum after exposure of the GI tract to an iron bolus (*54*) and in Caco2 cells, a model for enterocytes, after exposure of the apical surface to iron (*55*). This response could be regulatory or a physiological process participating in transcytosis of iron. With either explanation, one must also consider that the G185R mutation upsets the normal behavior resulting in loss or mislocalization of the transporter.

On the basis of these issues, we made immunoblots employing three isoform-specific antibodies to rat DMT1 in order to test for improper targeting. The +IRE form, previously considered to be the main form expressed on the apical surface of normal enterocytes, was enriched in BBM from *b*/*b* rats (Figure 7) as might be expected for their iron deficient state. The BBM levels of the −IRE species of DMT1 (Figure 8) and of isoforms containing exon 1A (Figure 9) also reflected the quantities in *b*/*b* duodenum. None of the three epitope-specific antibodies detected evidence of improper targeting after the G185R mutation, although the responses to iron deficiency varied depending on the isoform.

Thus our data from both immunoblots and microscopic localization (Figure 10) as well as independent immunohistochemical results (*53*) all imply that duodenal DMT1 is properly localized in rats after the G185R mutation. Hence the lack of detectable transport activity in *b*/*b* vesicles is not due to improper targeting of the transporter. Perhaps apparent incorrect targeting in the duodenum of *mk*/*mk* mice (*42*) could represent a failure to control for feeding and iron content of food (*54*). Nevertheless, there is evidence for altered targeting in *mk*/*mk* reticulocytes (*43*), kidney (*44*), and recently with an *mk* construct during ectopic expression (*46*). There are contrasting results available (*56*), indicating proper DMT1 localization in *b*/*b* reticulocytes. Data for *b*/*b* kidney (*57*) are consistent with altered targeting but complicated by dysmorphology of the mutant kidney. More data must accumulate, but the emerging picture is that the G185R mutation might affect subcellular localization in a tissue- and species-specific fashion. There are also some discrepancies between what is seen in confocal microscopy for the localization of isoforms and results after fractionation into BLM and BBM; for example, the level of the 1A isoform in the BLM fraction is higher than one might expect based on the fluorescent microscopy. These discrepancies probably reflect limitations in the fractionation technique.

BLMVs originating from the basolateral membranes of the duodenal extracts were also used to measure transport (Figure 5). These vesicles should be related to endosomal vesicles where there is also a loss of transport activity due to the G185R mutation (*3*, *5*, *11*). This assumption was consistent with the measurements indicating that +/*b* BLMV had comparable transport activity to BBMV and similar levels of each DMT1 species as detected in immunoblots. There were similar losses of activity in *b*/*b* vs +/*b* BLMV compared to their BBMV analogues (Figure 2). The residual quenching in *b*/*b* BLMV was about 20−25% of the active transport as in BBMV. Thus the mutant or active form of the protein is found in both membranes dependent on the genotype and independent of whether it is the +IRE, −IRE, or 1A transporter species (*1*, *3*, *35*, *58*). This conclusion is supported by the immunoblots (Figures 7−9) and fluorescent micrographs (Figure 10); the presence of distinct markers for the BBM in BBMV also confirms that BBMVs and BLMVs are distinct membrane preparations that contain DMT1 isoforms (Figure 6 and Table 2). The derived pseudo-first-order rate constants of the putative basolateral transport did not differ from those of BBMV. Overshoot in the loss of fluorescence intensity also occurs in the BLMV and again suggests a proton symport then re-equilibration of the vesicle cavity. While the BLMVs need to have fuller characterization to complete support of their origin from the BLM of enterocytes, the data in Figure 6 and Table 2 exclude substantial contamination from BBMV. Some of the BLMV DMT1 could originate from crypt cells, but these cells are not numerous enough to account for all of the DMT1, and

each isoform is found to some degree in the BLM in fluorescent micrographs (Figure 10) as noted above. The presence of DMT1 in BLM could indicate a role for the transporter in the enterocyte beyond the immediate uptake of metal ions at the BBM. This role could be in transcytosis, regulation of surface expression at the BBM, and uptake of iron from Tf to supply the enterocytes' needs during fasting or relate to metal ions other than iron. Alternatively, DMT1 in BLM could be a remnant of its presence there in the crypt cells that are the progenitors of enterocytes or the result of inaccuracy in targeting. Nevertheless, follow-up studies are needed to rule out alternative sources other than enterocytes for DMT1 in BLM and to support one or more of these roles.

Our results on enterocytes indicate that DMT1 is the activity assayed by the calcein-based assay and that *b*/*b* enterocytes are very deficient in that activity. Their deficiency is due to a functional deficit rather than an alteration in localization. DMT1 occurs in vesicles derived from both BBM and BLM. DMT1 in enterocytes may be primarily the +IRE isoforms, but the cells also contain 1A and −IRE isoform(s). Each isoform has a distinct distribution, possibly in support of multiple functions for the transporter.

ACKNOWLEDGMENT

We thank Mr. Kevin G. Dolan for expert technical assistance, Ms. Amy Johnson for instructing us on the fluorometer, and Dr. Agnieszka Lis for help with the protein assay. Drs. Jerome A. Roth and Laura Garrick kindly provided critical reviews of drafts.

REFERENCES

1. Gunshin, H., Mackenzie, B., Berger, U. V., Gunshin, Y., Romero, M. F., Boron, W. F., Nussberger, S., Gollan, J. L., and Hediger, M. A. (1997) Cloning and characterization of a mammalian proton-coupled metal-ion transporter, *Nature (London) 388*, 482−488.
2. Fleming, M. D., Trenor, C. I., Su, M. A., Foernzler, D., Beier, D. R., Dietrich, W. F., and Andrews, N. C. (1997) Microcytic anaemia mice have a mutation in *Nramp2*, a candidate iron transporter gene, *Nature Genet. 16*, 383−386.
3. Fleming, M. D., Romano, M. A., Su, M. A., Garrick, L. M., Garrick, M. D., and Andrews, N. C. (1998) *Nramp2* is mutated in the anemic Belgrade (*b*) rat: Evidence of a role for Nramp2 in endosomal iron transport, *Proc. Natl. Acad. Sci. U.S.A. 95*, 1148−1153.
4. Canonne-Hergaux, F., Gruenheid, S., Ponka, P., and Gros, P. (1999) Cellular and subcellular localization of the Nramp2 iron transporter in the intestinal brush border and regulation by dietary iron, *Blood 93*, 4406−4417.
5. Garrick, M. D., Gniecko, K., Liu, Y., Cohan, D. S., and Garrick, L. M. (1993) Transferrin and the transferrin cycle in Belgrade rat reticulocytes, *J. Biol. Chem. 268*, 14867−14874.
6. Gruenheid, S., Canonne-Hergaux, F., Gauthier, S., Hackam, D. J., Grinstein, S., and Gros, P. (1999) The iron transport protein NRAMP2 is an integral membrane glycoprotein that colocalizes with transferrin in recycling endosomes, *J. Exp. Med. 189*, 831−841.
7. Sladic-Simic, D., Pavic, D., Zivkovic, N., Marinkovic, D., and Martinovitch, P. N. (1963) Changes in the offspring of female rats exposed to 50 R of X-rays when eight days old, *Brit. J. Radiol. 36*, 542−543.
8. Sladic-Simic, D., Zivkovic, N., Pavic, D., Marinkovic, D., Martinovic, J., and Martinovitch, P. N. (1966) Hereditary hypochromic microcytic anemia in the laboratory rat, *Genetics 53*, 1079−1089.
9. Sladic-Simic, D., Martinovitch, P. N., Zivkovic, N., Pavic, D., Martinovic, J., Kahn, M., and Ranney, H. M. (1969) A thalassemic-like disorder in Belgrade laboratory rats, *Ann. N.Y. Acad. Sci. 165*, 93−99.
10. Garrick, L. M., Gniecko, K., Hoke, J. E., Al-Nakeeb, A., Ponka, P., and Garrick, M. D. (1991) Ferric-salicyaldehyde isonicotinoyl hydrazone, a synthetic iron chelate, alleviates defective iron utilization by reticulocytes of the Belgrade rat, *J. Cell. Physiol. 146*, 460−465.
11. Bowen, B. J., and Morgan, E. H. (1987) Anemia of the Belgrade rat: Evidence for defective membrane transport of iron, *Blood 70*, 38−44.
12. Garrick, L. M., Gniecko, K., Liu, Y., Cohan, D. S., Grasso, J. A., and Garrick, M. D. (1993) Iron distribution in Belgrade rat reticulocytes after inhibition of heme synthesis with succinylacetone, *Blood 81*, 3414−3421.
13. Garrick, M., Scott, D., Walpole, S., Finkelstein, E., Whitbred, J., Chopra, S., Trivikram, L., Mayes, D., Rhodes, D., Cabbagestalk, K., Oklu, R., Sadiq, A., Mascia, B., Hoke, J., and Garrick, L. (1997) Iron supplementation moderates but does not cure the Belgrade anemia, *BioMetals 10*, 65−76.
14. Farcich, E. A., and Morgan, E. H. (1992) Uptake of transferrin-bound and nontransferrin-bound iron by reticulocytes from the Belgrade laboratory rat: Comparison with Wistar rat transferrin and reticulocytes, *Am. J. Hematol. 39*, 9−14.
15. Garrick, L. M., Dolan, K. G., Romano, M. A., and Garrick, M. D. (1999) Nontransferrin-bound iron uptake in Belgrade and normal rat erythroid cells, *J. Cell. Physiol. 178*, 349−358.
16. Chua, A., and Morgan, E. H. (1997) Manganese metabolism is impaired in the Belgrade laboratory rat, *J. Comp. Physiol. B 167*, 361−369.
17. Russell, E. S., McFarland, E. C., and Kent, E. L. (1970) Low viability, skin lesions and reduced fertility associated with microcytic anemia in the mouse, *Transplant. Proc. 2*, 144−151.
18. Russell, E. S., Nash, D. J., Bernstein, S. E., Kent, E. L., McFarland, E. C., Matthews, S. M., and Norwood, M. S. (1970) Characterization and genetic studies of microcytic anemia in house mouse, *Blood 35*, 838−850.
19. Edwards, J. A., and Hoke, J. E. (1975) Red cell iron uptake in hereditary microcytic anemia, *Blood 46*, 381−388.
20. McKie, A. T., Barrow, D., Latunde-Dada, G. O., Rolfs, A., Sager, G., Mudaly, E., Mudaly, M., Richardson, C., Barlow, D., Bomford, A., et al. (2001) An iron-regulated ferric reductase associated with the absorption of dietary iron, *Science 291*, 1755−1759.
21. Knöpfel, M., and Solioz, M. (2002) Characterization of a Cytocrome b558 Ferric/Cupric Reductase from Rabbit Duodenal Brush Border Membranes, *Biochem. Biophys. Res. Commun. 291*, 220−225.
22. Abboud, S., and Haile, D. J. (2000) A novel mammalian iron-regulated protein involved in intracellular iron metabolism, *J. Biol. Chem. 275*, 19906−19912.
23. Donovan, A., Brownlie, A., Zhou, Y., Shepard, J., Pratt, S. J., Moynihan, J., Paw, B. H., Drejer, A., Barut, B., Zapata, A., Peters, T. J., Raja, K. B., Shirali, S., Hediger, M. A., Farzaneh, F., and Simpson, R. J. (2000) Positional cloning of zebrafish ferroportin1 identifies a conserved vertebrate iron exporter, *Nature (London) 403*, 776−781.
24. McKie, A. T., Marciani, P., Rolfs, A., Brennan, K., Wehr, K., Barrow, D., Miret, S., Bomford, A., Peters, T. J., Farzaneh, F., et al. (2000) A novel duodenal iron-regulated transporter, IREG1, implicated in the basolateral transfer of iron to the circulation, *Mol. Cell 5*, 299−309.
25. Vulpe, C. D., Kuo, Y. M., Murphy, T. L., Cowley, L., Askwith, C., Libina, N., Gitschier, J., and Anderson, G. J. (1999) Hephaestin, a ceruloplasmin homologue implicated in intestinal iron transport, is defective in the *sla* mouse, *Nature Genet. 21*, 195−199.
26. Yoshida, K., Furihata, K., Takeda, S., Nakamura, A., Yamamoto, K., Morita, H., Hiyamuta, S., Ikeda, S., Shimizu, N., and Yanagisawa, N. (1995) A mutation in the ceruloplasmin gene is associated with systemic hemosiderosis in humans, *Nature Genet. 9*, 267−272.
27. Conrad, M. E., Umbreit, J. N., Moore, E. G., Hainsworth, L. N., Porubcin, M., Simovich, M. J., Nakada, M. T., Dolan, K., and Garrick, M. D. (2000) Separate pathways for cellular uptake of ferric and ferrous iron, *Am. J. Physiol. Gastrointest. Liver Physiol. 279*, G767−G774.
28. Worthington, M. T., Cohn, S. M., Miller, S. K., Luo, R. Q., and Berg, C. L. (2001) Characterization of a human plasma membrane heme transporter in intestinal and hepatocyte cell lines, *Am. J. Physiol. Gastrointest. Liver Physiol. 280*, G1172−G1177.
29. Su, M. A., Trenor, C. I., Fleming, J. C., Fleming, M. D., and Andrews, N. C. (1998) The G185R mutation disrupts functions of the iron transporter Nramp2, *Blood 92*, 2157−2163.

30. Worthington, M. T., Browne, L., Battle, E. H., and Luo, R. Q. (2000) Functional properties of transfected human DMT1 iron transporter, *Am. J. Physiol. Gastrointest. Liver Physiol. 279*, G1265−G1273.
31. Garrick, M. D., and Dolan, K. G. (2002) An Expression System for a Transporter of Iron and Other Metals, in *Ultrastructure and Molecular Biology Protocols for Oxidant and AntiOxidants, Methods in Molecular Biology* (D. Armstrong, Ed.) pp 147−154, Humana, Totawa.
32. Knöpfel, M., Schulthess, G., Funk, F., and Hauser, H. (2000) Characterization of an integral protein of the brush border membrane mediating the transport of divalent metal ions, *Biophys. J. 79*, 874−884.
33. Garrick, M. D., Dolan, K. G., Ghio, A., Horbinski, C., Higgins, D., Porubcin, M., Moore, E. G., Hainsworth, L. N., Umbreit, J. N., Conrad, M. E., Feng, L., Lis, A., Roth, J. E., Singleton, S., and Garrick, L. M. (2003) DMT1 (Divalent Metal Transporter 1): A mammalian transporter for multiple metals, *BioMetals 16*, 41−54.
34. Roth, J. A., Horbinski, C., Feng, L., Dolan, K. G., Higgins, D., and Garrick, M. D. (2000) Differential localization of divalent metal transporter 1 with and without iron response element in rat PC12 and sympathetic neuronal cells, *J. Neurosci. 20*, 7595−7601.
35. Hubert, N., and Hentze, M. W. (2002) Previously uncharacterized isoforms of divalent metal transporter (DMT)-1: Implications for regulation and cellular function, *Proc. Natl. Acad. Sci. U.S.A. 99*, 12345−12350.
36. Kuo, H. C., Smith, J. J., Lis, A., Zhao, L., Gonsiorek, E. A., Zhou, X., Higgins, D. M., Roth, J. A., Garrick, M. D., and Garrick, L. (2004) A computer-identified nuclear localization signal in exon 1A of the transporter DMT1 is essentially ineffective in nuclear targeting, *J. Neurosci. Res. 76*, 497−511.
37. Knoepfel, M., and Garrick, M. D. (2002) Absence of divalent metal ion transport activity in vesicles from the duodenum of Belgrade rats, *Blood 100*, 6b.
38. Garrick, M. D., Zhao, L., and Knöpfel, M. (2003) G185R-mutated DMT1 remains in both brush border and basolateral vesicles from the duodenum of Belgrade rats, *Blood 102*, 755a.
39. Flint, N., Cove, F. L., and Evans, G. S. (1991) A low-temperature method for the isolation of small-intestinal epithelium along the crypt-villus axis, *Biochem. J. 280*, 331−334.
40. Smith, P. K., Krohn, R. I., Hermanson, G. T., Mallia, A. K., Gartner, F. H., Provenzano, M. D., Fujimoto, E. K., Goeke, N. M., Olson, B. J., and Klenk, D. C. (1985) Measurement of protein using bicinchonic acid, *Anal. Biochem. 150*, 76−85.
41. Edwards, J. A., Garrick, L. M., and Hoke, J. E. (1978) Defective iron uptake and globin synthesis by erythroid cells in the anemia of the Belgrade laboratory rat, *Blood 51*, 347−357.
42. Canonne-Hergaux, F., Fleming, M. D., Levy, J. E., Gauthier, S., Ralph, T., Picard, V., Andrews, N. C., and Gros, P. (2000) The Nramp2/DMT1 iron transporter is induced in the duodenum of microcytic anemia *mk* mice but is not properly targeted to the intestinal brush border, *Blood 96*, 3964−3970.
43. Canonne-Hergaux, F., Zhang, A. S., Ponka, P., and Gros, P. (2001) Characterization of the iron transporter DMT1 (NRAMP2/DCT1) in red blood cells of normal and anemic *mk*/*mk* mice, *Blood 98*, 3823−3830.
44. Canonne-Hergaux, F. S., and Gros, P. (2002) Expression of the iron transporter DMT1 in kidney from normal and anemic *mk* mice, *Kidney Int. 62*, 147−156.
45. Xu, H., Jin, J., DeFelice, J. L., Andrews, N. C., and Clapham, D. E. (2004) A spontaneous, recurrent mutation in Divalent Metal Transporter-1 exposes a calcium entry pathway, *PLoS Biology 2*, 0378−0385.
46. Touret, N., Martin-Orozco, N., Paroutis, P., Furuya, W., Lam-Yuk-Tseung, S., Forbes, J., Gros, P., and Grinstein, S. (2004) Molecular and cellular mechanisms underlying iron transport deficiency in microcytic anemia, *Blood 140*, 1526−1533.
47. Garrick, M. D., and Garrick, L. M. (2004) in *Membrane Transporter Diseases* (Broer, S., and Wagner, C., Eds.) pp 107−122, Kluwer, Dordrecht.
48. Park, J. D., Cherrington, N. J., and Klaassen, C. D. (2002) Intestinal absorption of cadmium is associated with Divalent Metal Transporter 1 in rats, *Toxicol. Sci. 68*, 288−294.
49. Bannon, D. I., Portnoy, M. E., Olivi, L., Lees, P., Culotta, V. C., and Bressler, J. P. (2002) Uptake of lead and iron by divalent metal transporter 1 in yeast and mammalian cells, *Biochem. Biophys. Res. Commun. 295*, 978−984.
50. Arredondo, M., Munoz, P., Mura, C. V., and Nunez, M. T. (2003) DMT1, a physiologically relevant apical Cu^{1+} transporter of intestinal cells, *Am. J. Physiol. Cell Physiol. 284*, C1525−C1530.
51. Llanos, R. M., and Mercer JF (2002) The molecular basis of copper homeostasis copper-related disorders, *DNA Cell Biol. 21*, 259−270.
52. Cragg, R. A., Christie, G. R., Phillips, S. R., Russi, R. M., Kury, S., Mathers, J. C., Taylor, P. M., and Ford, D. (2002) A novel zinc-regulated human zinc transporter, hZTL1, is localized to the enterocyte apical membrane, *J. Biol. Chem. 277*, 22789−22797.
53. Morgan, E. H., and Oates, P. S. (2002) Mechanisms and regulation of intestinal iron absorption, *Blood Cells Mol. Dis. 29*, 384−399.
54. Yeh, K. Y., Yeh, M., Watkins, J. A., Rodriguez, P. J., and Glass, J. (2000) Dietary iron induces rapid changes in rat intestinal divalent metal transporter expression, *Am. J. Physiol. Gastrointest. Liver Physiol. 279*, G1070-G1079.
55. Ma, Y. X., Specian, R. D., Yeh, K. Y., Yeh, M., Rodriguez, P. J., and Glass, J. (2002) The transcytosis of divalent metal transporter 1 and apo-transferrin during iron uptake in intestinal epithelium, *Am. J. Physiol. Gastrointest. Liver Physiol. 283*, G965−G974.
56. Garrick, M. D., Fletcher, R. J., Dolan, K. G., Romano, M. A., Walowitz, J., Roth, J. A., Umbreit, J. N., Conrad, M. E., and Garrick, L. M. (1999) The iron transporter DMT1 (or Nramp2 or DCT1) is located mostly in endosomes in normal and Belgrade rat reticulocytes, *Blood 94*, 403a.
57. Ferguson, C. J., Wareing, M., Delannoy, M., Fenton, R., McLarnon, S. J., Ashton, N., Cox, A. G., McMahon, R., Garrick, L. M., Green, R., Smith, C. P., and Riccardi, D. (2003) Iron handling and gene expression of the divalent metal transporter, DMT1, in the kidney of the anemic Belgrade (*b*) rat, *Kidney Int. 64*, 1755−1764.
58. Lee, P. L., Gelbart, T., West, C., Halloran, C., and Beutler, E. (1998) The human Nramp2 gene: Characterization of the gene structure, alternative splicing, promoter region and polymorphisms, *Blood Cells Mol. Dis. 24*, 199−215.

BI048768+